Supplementary Information for:

Identification of evolutionary and kinetic drivers of NAD-dependent signalling

Mathias Bockwoldt[1], Dorothée Houry[2], Marc Niere[3], Toni I. Gossmann[4,5], Ines Reinartz[6,7], Alexander Schug[8], Mathias Ziegler[3], and Ines Heiland[1,§]

[1]Department of Arctic and Marine Biology, UiT The Arctic University of Norway, Biologibygget, Framstredet 39, 9017 Tromsø, Norway
[2]Department of Biological Sciences, University of Bergen, Thormøhlens gata 53 A/B, 5006 Bergen, Norway
[3]Department of Biomedicine, University of Bergen, Jonas Lies vei 91, 5009 Bergen, Norway
[4]Department of Animal and Plant Sciences, Western Bank, University of Sheffield, Sheffield, S10 2TN, United Kingdom
[5]Department of Animal Behaviour, Bielefeld University, 33501 Bielefeld, Germany
[6]Department of Physics, Karlsruhe Institute of Technology, Wolfgang-Gaede-Str. 1, 76131 Karlsruhe, Germany
[7]Steinbuch Centre for Computing, Karlsruhe Institute of Technology, Hermann-von-Helmholtz-Platz 1, 76344 Eggenstein-Leopoldshafen, Germany
[8]John von Neumann Institute for Computing, Jülich Supercomputing Centre, Forschungszentrum Jülich, 52425 Jülich, Germany
§ Corresponding author: ines.heiland@uit.no

This PDF file includes:

Figures S1 to S9
Tables S1 to S4

Other supplementary materials for this manuscript include the following:

Scripts used to run the phylogenetic analysis are available here:
https://github.com/MolecularBioinformatics/Phylogenetic-analysis
The SBML files of the mathematical models used for the pathway simulations in figures 3, 4, 6, S3 and S6 are accessible through the Biomodels database (https://www.ebi.ac.uk/biomodels/models) acession no. MODEL1905220001 and MODEL1905220002.

www.pnas.org/cgi/doi/10.1073/pnas.1902346116

Figure S1

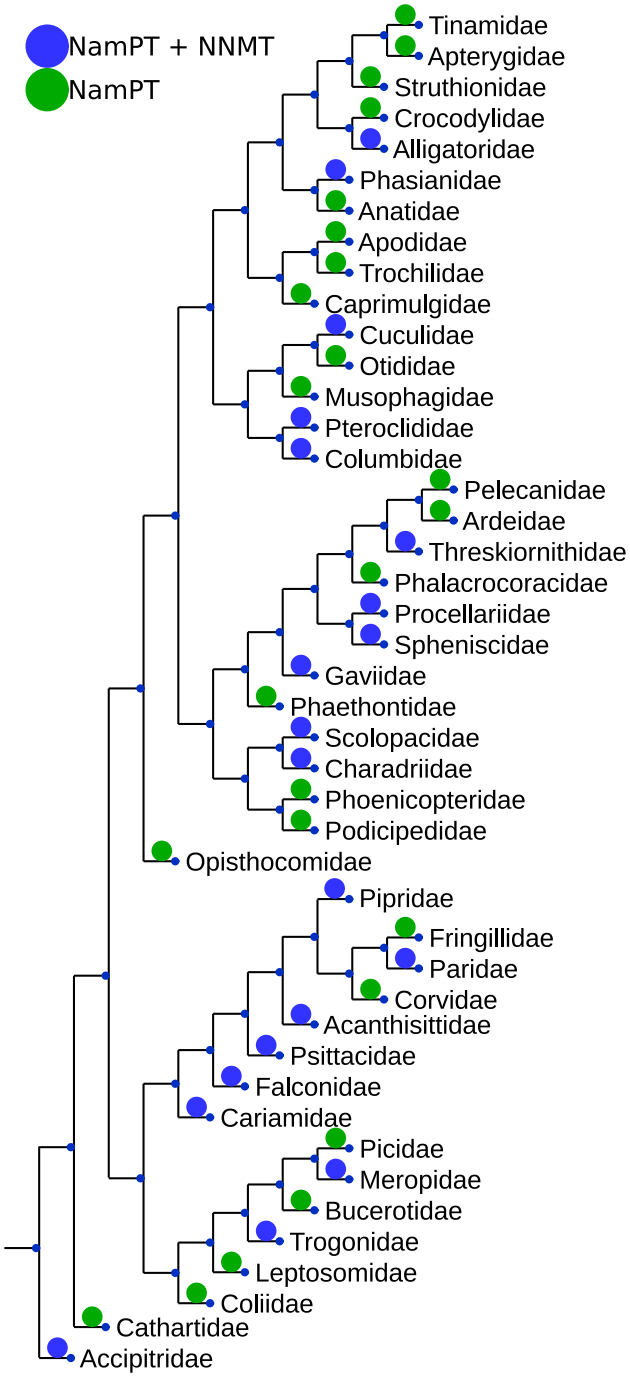

The phylogenetic distribution of NamPT and NNMT in birds and reptiles is scattered. The phylogenetic distribution of birds and reptiles was adopted from Prum et al. 2015 [1]. Families are marked with a green circle if they possess NamPT without NNMT or a blue circle if they possess both NamPT and NNMT.

Figure S2

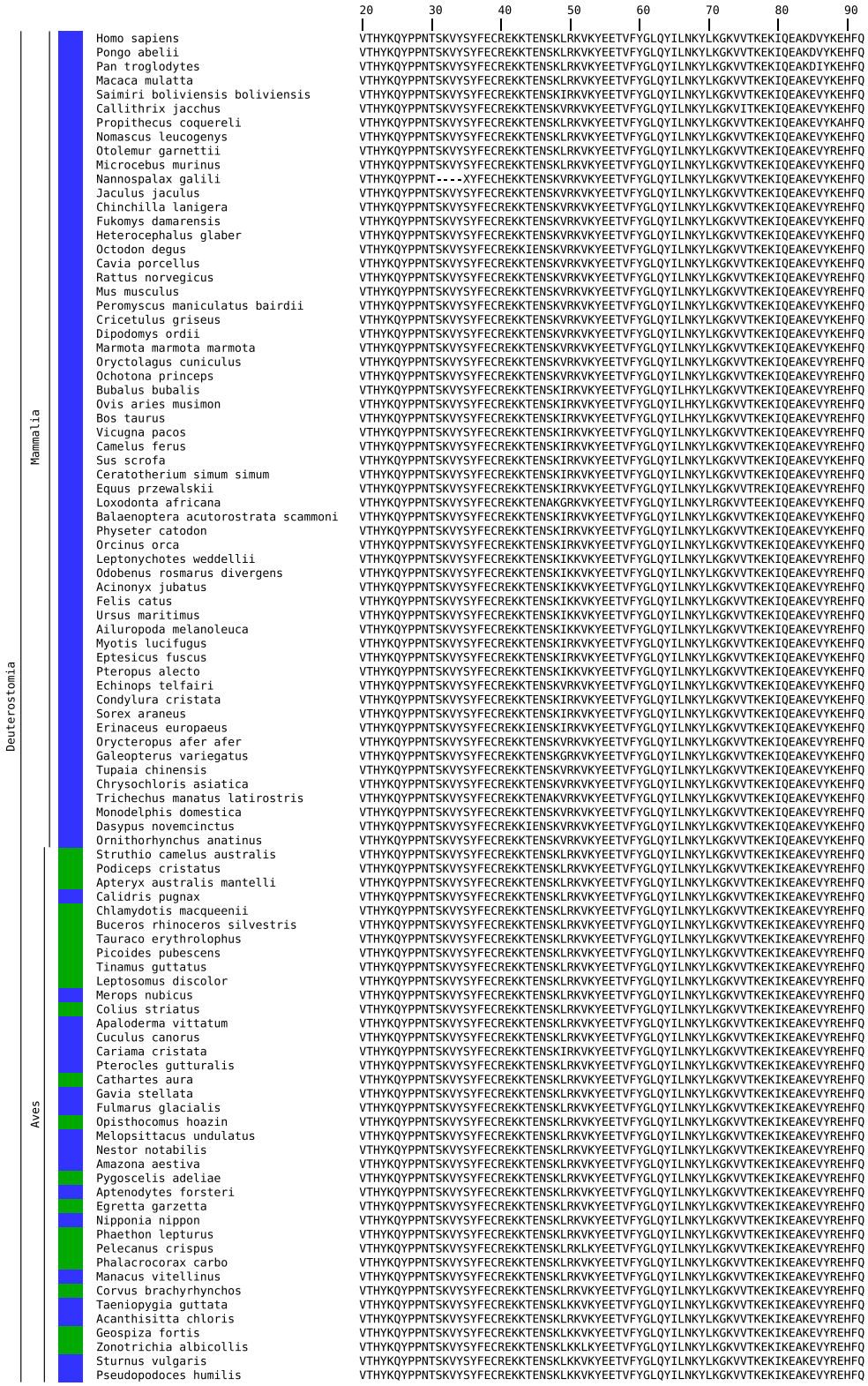

Continued at next page.

Figure S2 continued

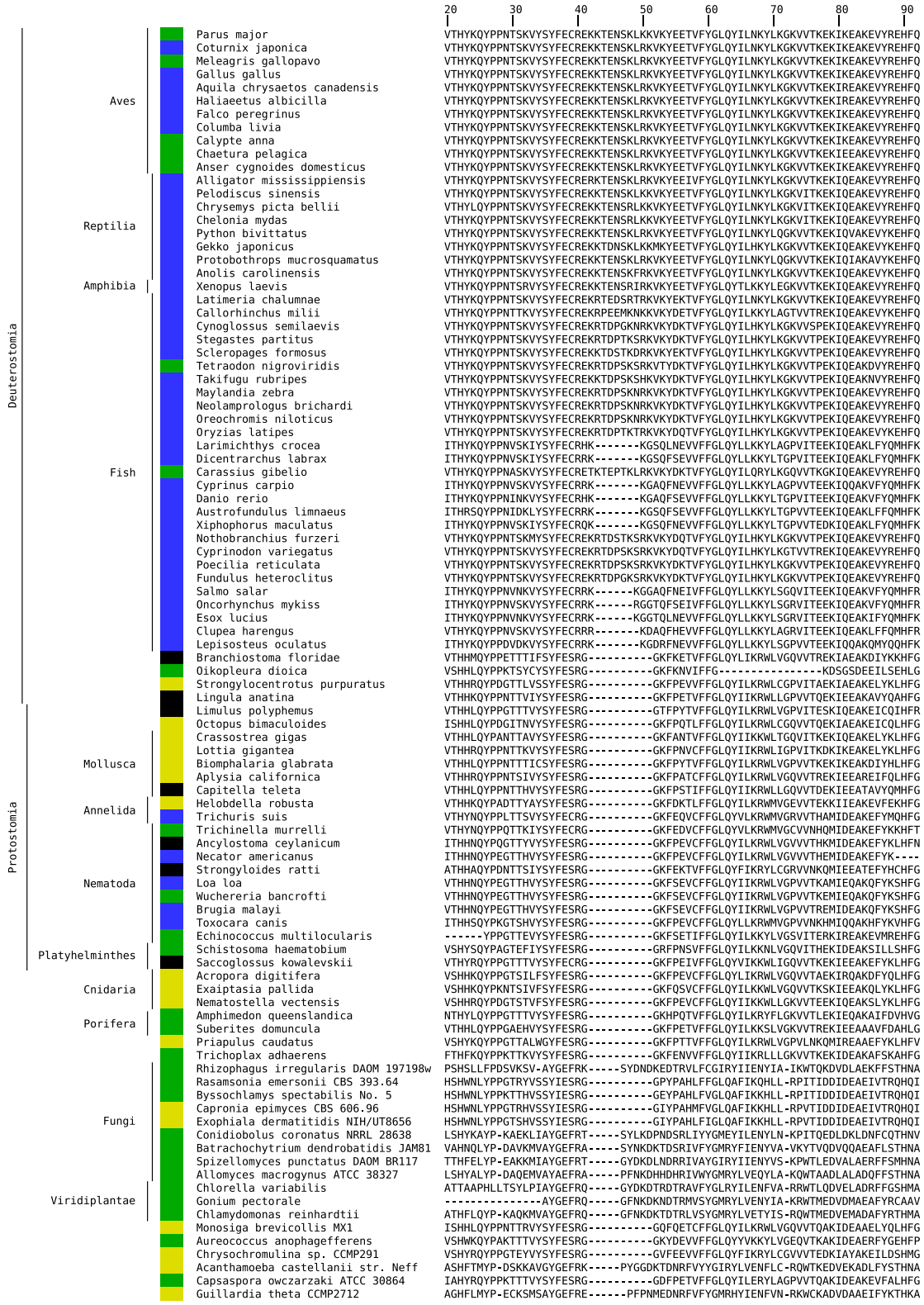

The structurally unresolved loop of NamPT. Sequence alignment of NamPT of different species cropped to the region around the unresolved loop structure.

Figure S3

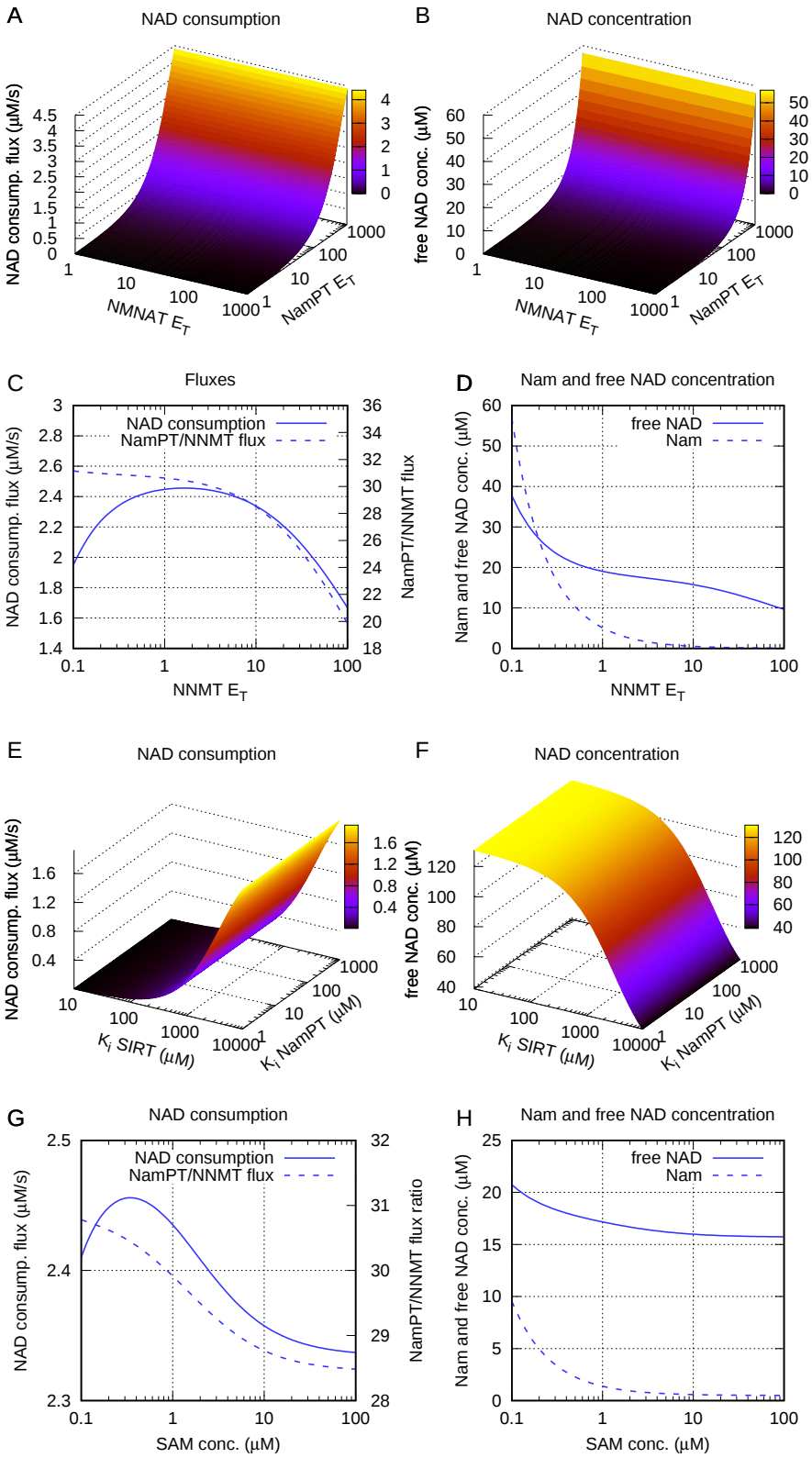

Influence of enzyme expression, SAM concentration and inhibition constants on systems behaviour. We used the dynamic model of NAD biosynthesis and consumption to analyse the effect of NMNAT, NamPT (A and B) and NNMT (C and D) expression on NAD consumption flux (A and C) and free NAD concentration (B and D), NamPT/NNMT flux ratio (C) and Nam concentration (D). We furthermore varied the inhibition constants $K_i(Nam)$ and $K_i(NAD)$ for SIRT1 and NamPT, respectively, in a model without NNMT (E and F). This mimics the potential effect of inhibition relaxation due to reduced Nam or NAD concentrations. In addition, we simulated the effect of changes in the NNMT cofactor S-adenosyl methionine (SAM) on NAD consumption flux, NamPT/NNMT flux ratio (G), Nam and free NAD concentration (H).

Figure S4

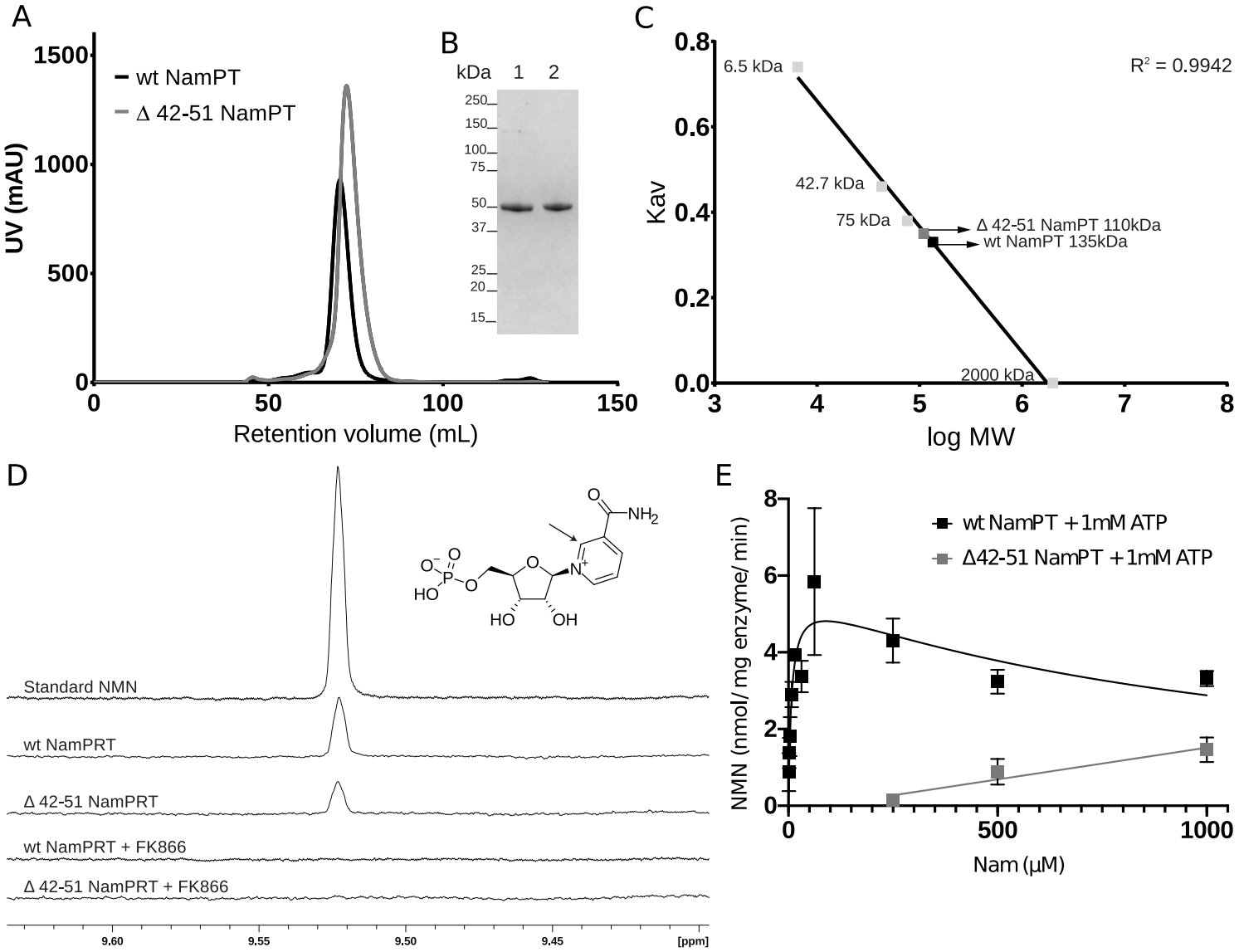

Purification of wildtype NamPT and Δ42-51 NamPT, NMR spectra and NamPT substrate affinity measurements A) Elution profile of wildtype (wt) and Δ42-51 NamPT on size-exclusion chromatography using a Superdex 200 16/60 column. B) Coomassie stained denaturating SDS-PAGE analysis of Δ42-51 NamPT (lane 1) and wt NamPT (lane 2). 3 μg of pooled enzyme eluted from SEC was loaded onto the gel. C) The column was calibrated with apronitin 6.5 kDa, ovalbumine 42.7 kDa, coalbumine 75 kDa and blue dextran 2000 kDa. The partition coefficient (Kav) was determined for each standard (light grey squares) and plotted versus $\log_{10}$ molecular weight. The apparent molecular weight of wt NamPT and Δ42-51 NamPT was calculated to be 135 kDa and 110 kDa, respectively. D) Exemplary 1D 1H NMR NMR spectra of NMN formation used to quantify the activity of wildtype and mutant NamPT. Inset: molecular structure of NMN with the atom detected by NMR indicated by an arrow. The range used for NMN detection in typical 1D-1H-NMR spectra of the enzymatic reactions is shown. Samples and standards were supplemented with 1mM of DSS as internal standard. NMN quantification was done with the singlet detected at 9.52 ppm. From the top to the bottom, peak detection of NMN standard (200 µM), wt NamPT (1 mM Nam and 1 mM PRPP), Δ42-51 NamPT (1 mM Nam and 1 mM PRPP), wildtype NamPT with FK866, and Δ42-51 NamPT with FK866. Incubation with inhibitor FK866 was done for 30 min at 30 °C. E) To compare the substrate affinity of wtNamPT and Δ42-51 NamPT, 2 μM enzyme were incubated for 5 min at 30 °C with 1mM ATP and PRPP and 1μM to 1mM Nam in 300µl reaction buffer (20mM Tris-HCl pH 8.0, 500mM NaCl, 6mM MgCl2, 0.03% (w/v) BSA). Reaction was stopped with 100µM of FK866 and frozen in liquid nitrogen. The protein was removed using Amicon Ultra Centrifugal Filters (Millipore - 10 kDa cut-off). NMN formation was measured by LC-MS using an LC Dionex Ultimate 3000 instrument coupled to a Q Exactive Orbitrap mass spectrometer (Thermo Scientific). For LC separation, an Ascentis Express C18, (10 cm x 2.1mM, particle size 2.7 µm) column was used (Sigma-Aldrich) with a stepwise gradient form 10 mM ammonium acetate pH 5 and 2 mM tetrabutylammonium bromide (TBAB) to 10 mM ammonium acetate pH 6.8, 2 mM TBAB and 90% acetonitrile at a flow rate of $0.4\frac{ml}{min}$. Electrospray was used as ionization source, and samples were analysed in positive mode. Xcalibur software (Thermo Scientific, Waltham, MA, USA) was used for data visualization and peak integration. NMN meassurement data are available at: https://doi.org/10.15490/fairdomhub.1.datafile.2944.1

Figure S5

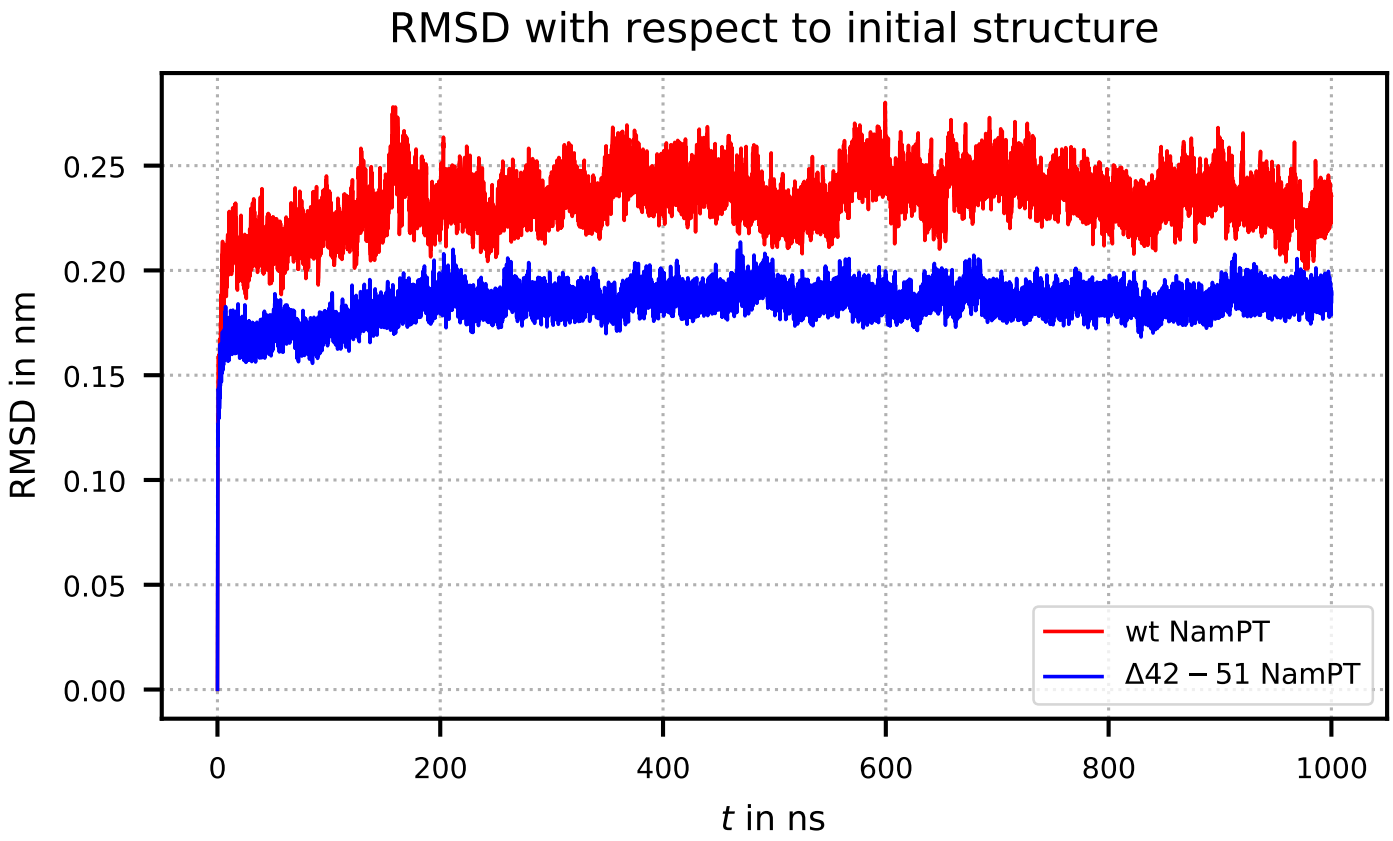

Molecular dynamics simulations NamPT. Root mean square deviation (RMSD) with respect to initial structure for simulation of wildtype (wt) NamPT (red) and mutant Δ42-51 NamPT (blue), respectively. The RMSD values for the entire simulation (in total 1000 ns) show stable structures with small fluctuations.

Figure S6

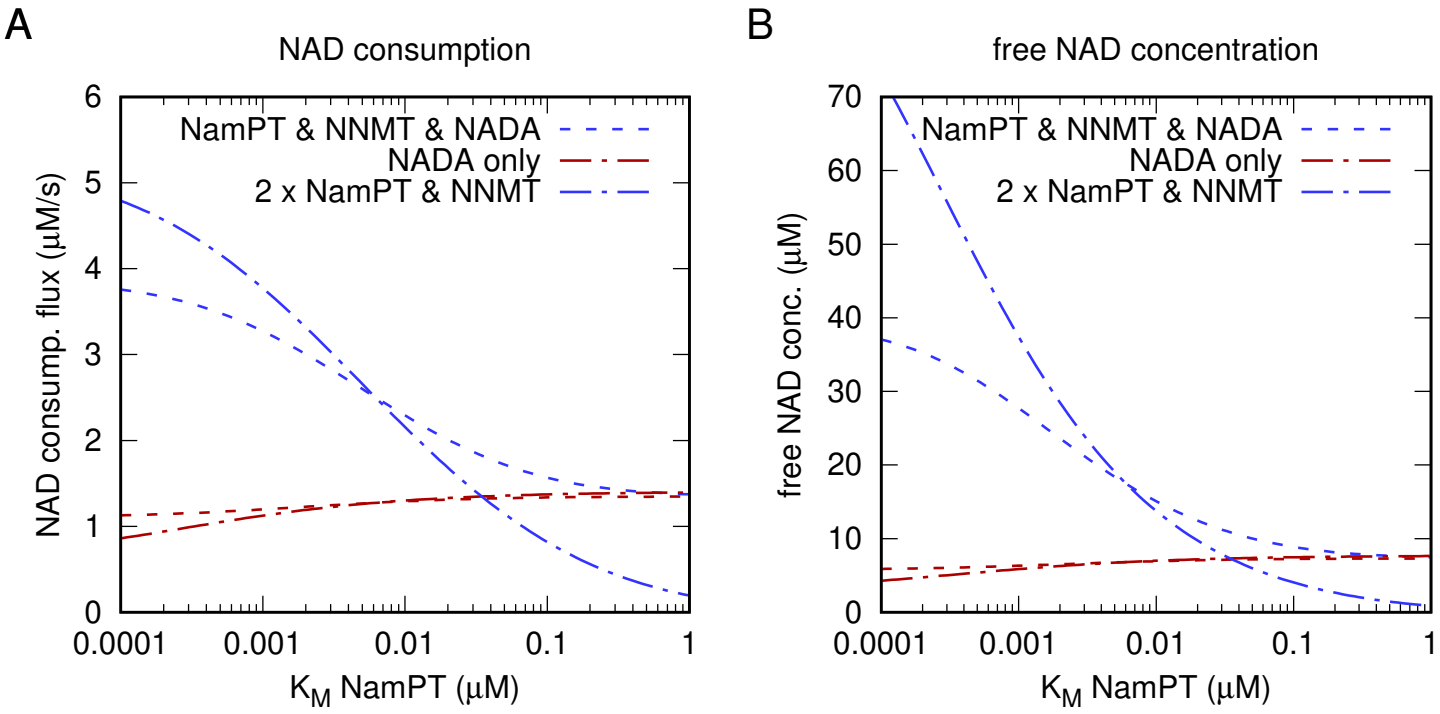

Potential impact of NADA on the evolution of high affinity NamPT. We simulated competition between two compartments, one containing only NADA (red lines) and one containing either NamPT, NADA and NNMT or twice the amount of NamPT to keep the sum of the amount of NADA+NamPT constant between simulations. As can be seen, the addition of NADA to NNMT and a low affinity NamPT, provides a slight advantage for A) NAD consumption flux and B) NAD concentration over NADA alone. As soon as the affinity of NamPT is high enough, double amounts of NamPT together with NNMT outcompete the combination of all three enzymes. The fact that this latter combination is actually found in some invertebrates might indicate that there is indeed an advantage over NADA alone.

Figure S7

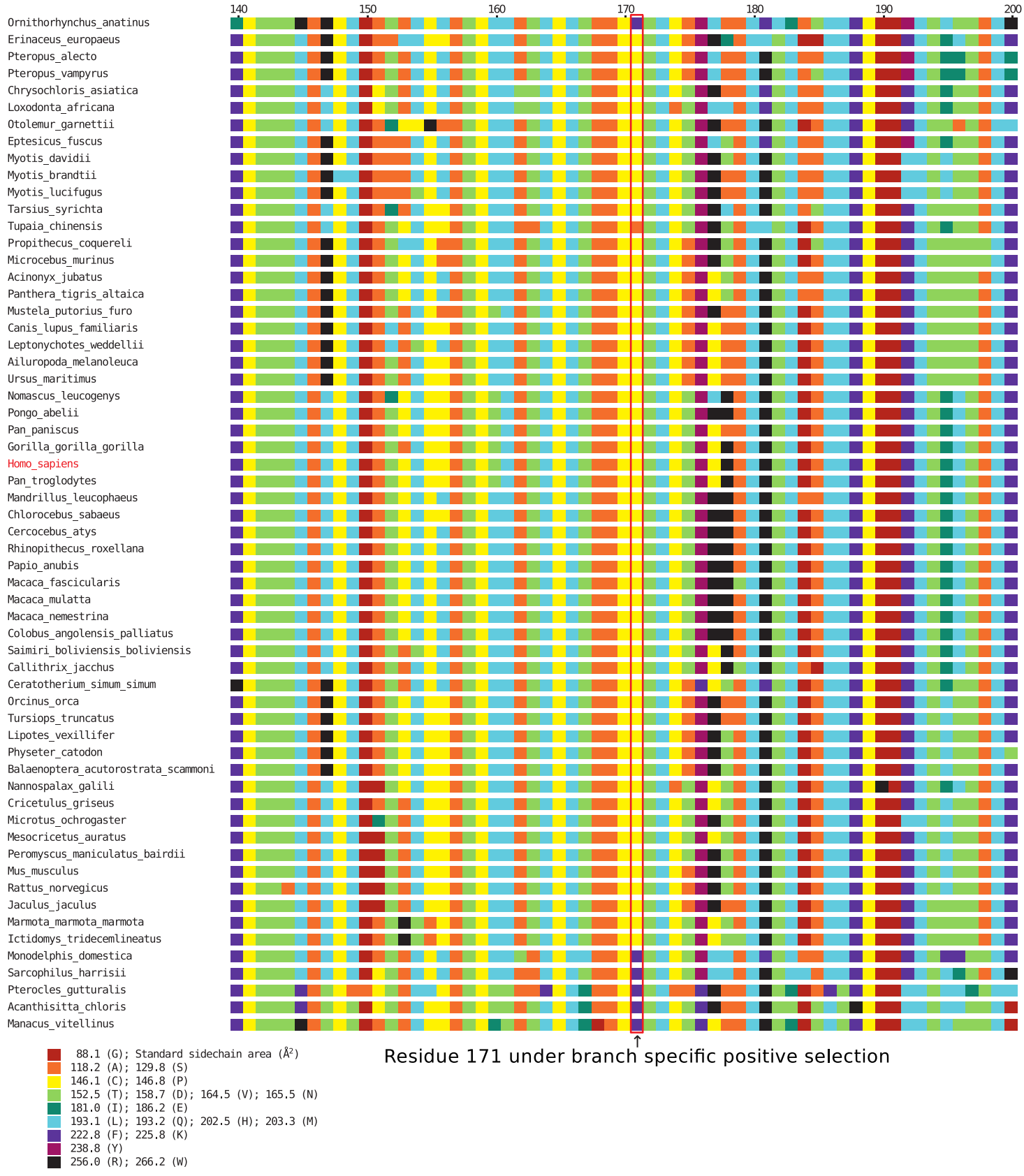

Site specific positive selection in NNMT Branch specific test of positive selection conducted for NNMTs from various vertebrate species reveals a signature of positive selection specific to residue 171 occurring at the lineage leading to placentalia. Shown is a cropped fingerprint alignment using biochemical colour-coding for NNMTs of the species under consideration with the critical residue 171 indicated. Underlying statistics and tree are shown in Supplementary Figure S8.

Figure S8

A

Branch site model A with foreground ω 2a/b fixed=1

site class	0	1	2a	2b
proportion	0.79326	0.17431	0.02659	0.00584
background ω	0.10465	1.00000	0.10465	1.00000
foreground ω	0.10465	1.00000	1.00000	1.00000

loglikelihood = -11145.741592

Branch site model A

site class	0	1	2a	2b
Proportion	0.81062	0.17848	0.00893	0.00197
background ω	0.10492	1.00000	0.10492	1.00000
foreground ω	0.10492	1.00000	33.95277	33.95277

loglikelihood = -11143.403032

2xDIFF = 4.68 (p < 0.05, χ2, d.f. = 1)

Site of interests (NEB)

171 K 0.983*

B

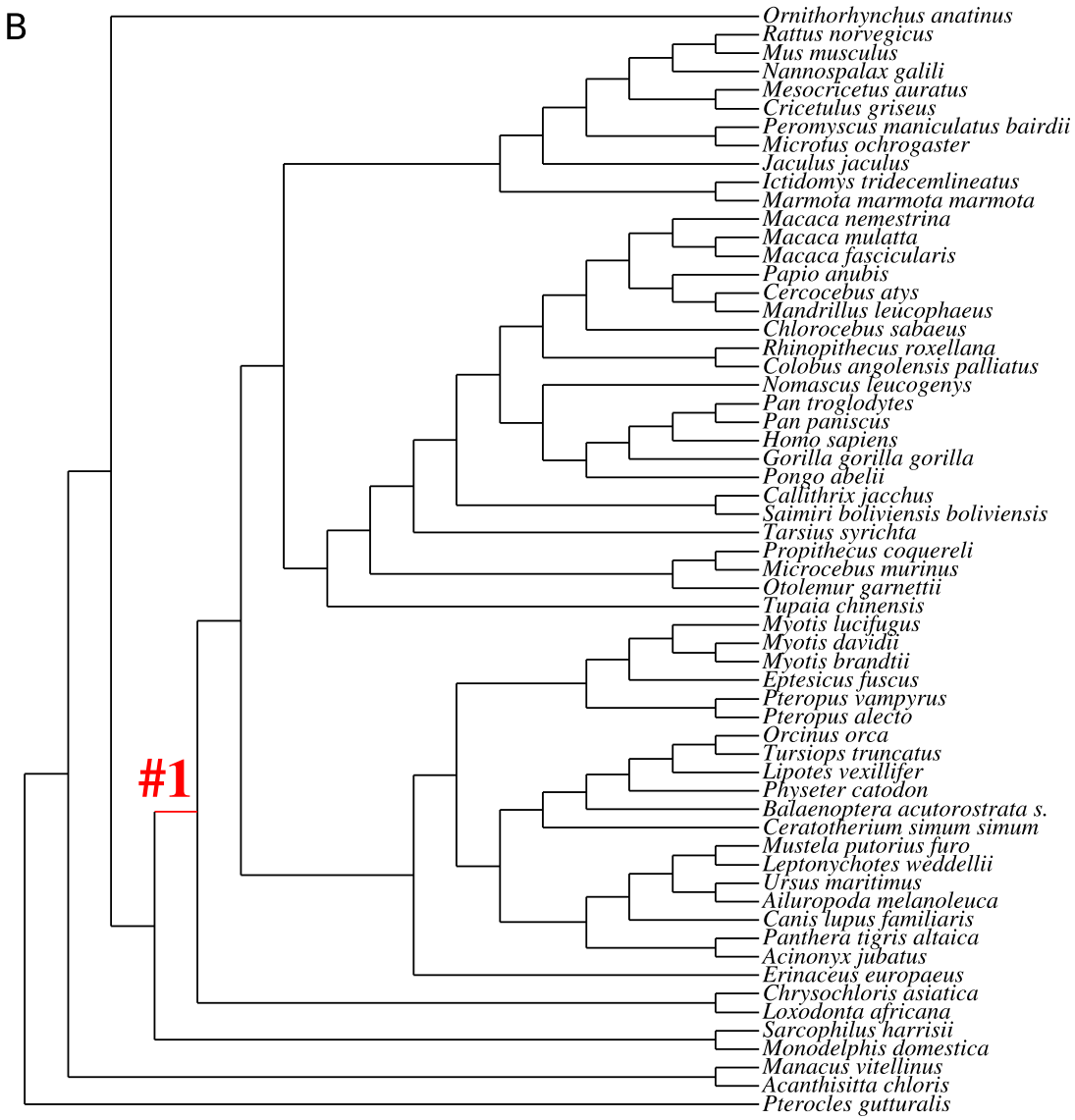

Site specific positive selection in NNMT Branch specific test of positive selection conducted for NNMTs from various vertebrate species reveals a signature of positive selection specific to residue 171 occurring at the lineage leading to placentalia. A) Output of the codeml runs (Branch-site model A of positive selection), the likelihood between a model with no positive selection ($\omega 2a/b = 1$) is compared to a model with positive selection ($\omega 2a/b > 1$). Significance between the two models is assessed using a likelihood ratio test assuming that twice the likelihood difference is χ^2 distributed. The critical value is 3.84 at the 5% level. B) The underlying tree topology for the codeml runs including the tested branch indicated with #1. The alignment is shown in Supplementary Figure S7.

Figure S9

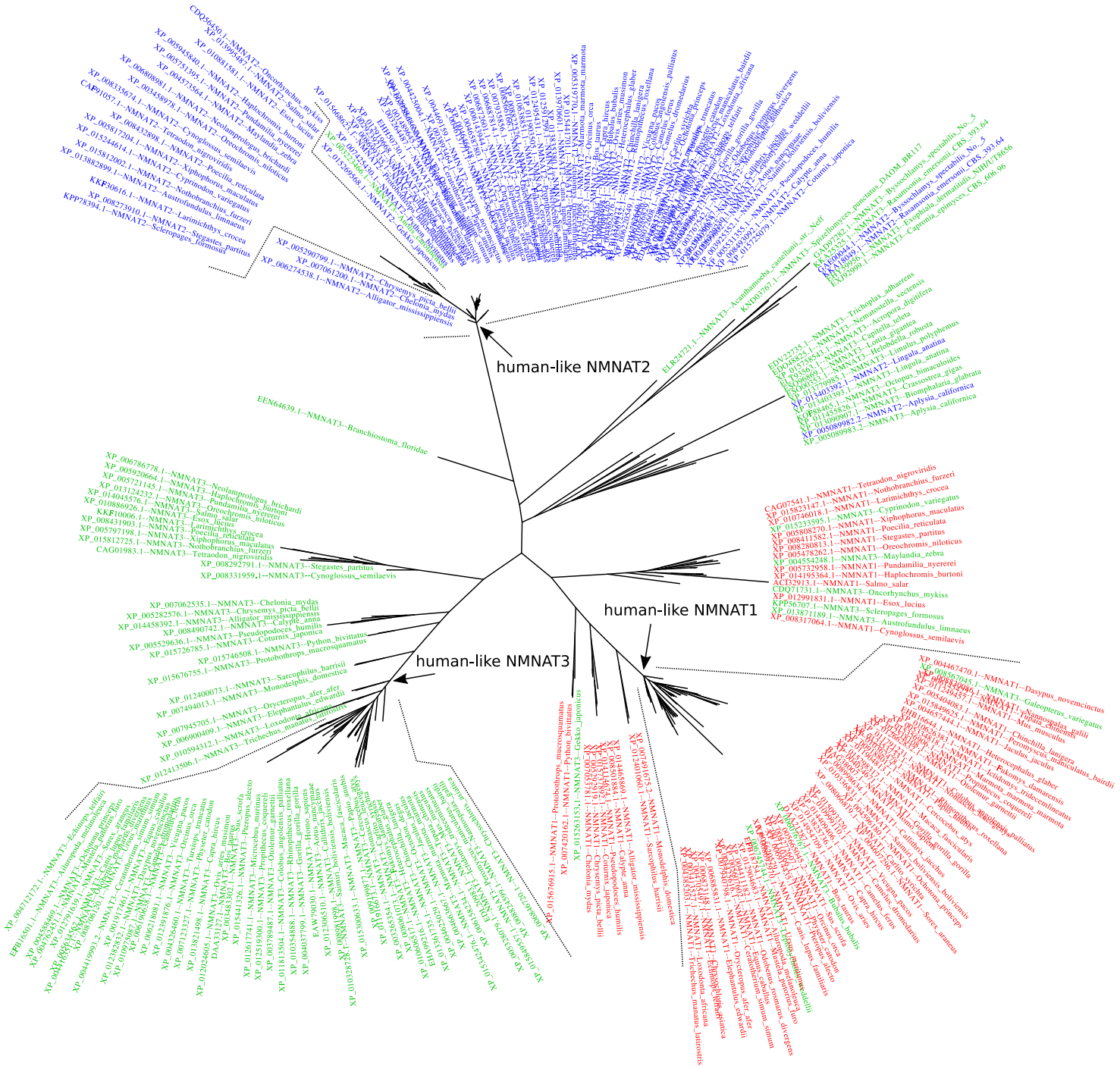

Clustering of NMNAT protein sequences of various eukaryotic species. Protein sequences were found using protein Blast with the human sequences as seeds. Protein names in red, blue, and green were found with the lowest expect value with the human NMNAT1, 2, and 3, respectively. Clustering was done with BAli-Phy version 3.0 (Suchard and Redeling 2006). The tree was visualised with Figtree version 1.4.3 (http://tree.bio.ed.ac.uk/software/figtree). Names were spread manually and dotted lines were added for better readability.

Table S1

#	Enzyme group	Gene name	Enzyme name	EC number	Uniprot ID	Species	Min. length
1	ADPRcyc	CD38	ADP-ribosyl cyclase/cyclic ADP-ribose hydrolase 1	3.2.2.6	P28907	*H. sapiens*	200
2	ADPRcyc	BST1	ADP-ribosyl cyclase/cyclic ADP-ribose hydrolase 2	3.2.2.6	Q10588	*H. sapiens*	200
3	ART	ART1	GPI-linked NAD(P)(+)--arginine ADP-ribosyltransferase 1	2.4.2.31	P52961	*H. sapiens*	200
4	ART	ART3	Ecto-ADP-ribosyltransferase 3	2.4.2.31	Q13508	*H. sapiens*	200
5	ART	ART4	Ecto-ADP-ribosyltransferase 4	2.4.2.31	Q93070	*H. sapiens*	200
6	ART	ART5	Ecto-ADP-ribosyltransferase 5	2.4.2.31	Q96L15	*H. sapiens*	200
14	NADA	NIC1	Nicotinamidase 1	3.5.1.19	Q8S8F9	*A. thaliana*	170
15	NADA	pnc-1	Pyrazinamidase and NiCotinamidase	3.5.1.19	Q9N426	*C. elegans*	170
16	NADA	pncA	Pyrazinamidase/nicotinamidase	3.5.1.19	P21369	*E. coli*	170
17	NADA	PNC1	Nicotinamidase	3.5.1.19	P53184	*S. cerevisiae*	170
25	NamPT	NPT1	Nicotinamide phosphoribosyltransferase	2.4.2.12	D9I2J1	*C. reinhardtii*	400
26	NamPT	NAMPT	Nicotinamide phosphoribosyltransferase	2.4.2.12	P43490	*H. sapiens*	400
38	NNMT	B0303.2	Uncharacterized methyltransferase	2.1.1.-	P34254	*C. elegans*	150
39	NNMT	NNMT	Nicotinamide N-methyltransferase	2.1.1.1	P40261	*H. sapiens*	150
40	PARP1-3	PARP1	Poly [ADP-ribose] polymerase 1	2.4.2.30	Q9ZP54	*A. thaliana*	300
41	PARP1-3	PARP2	Poly [ADP-ribose] polymerase 2	2.4.2.30	Q11207	*A. thaliana*	300
42	PARP1-3	PARP3	Poly [ADP-ribose] polymerase 3	2.4.2.30	Q9FK91	*A. thaliana*	300
43	PARP1-3	pme-1	Poly(ADP-ribose) polymerase	2.4.2.30	Q9N4H4	*C. elegans*	300
44	PARP1-3	pme-2	Poly(ADP-ribose) polymerase	2.4.2.30	Q09525	*C. elegans*	300
45	PARP1-3	PARP1	Poly [ADP-ribose] polymerase 1	2.4.2.30	P09874	*H. sapiens*	300
46	PARP1-3	PARP2	Poly [ADP-ribose] polymerase 2	2.4.2.30	Q9UGN5	*H. sapiens*	300
47	PARP1-3	PARP3	Poly [ADP-ribose] polymerase 3	2.4.2.30	Q9Y6F1	*H. sapiens*	300
48	PARP4	PARP4	Poly [ADP-ribose] polymerase 4	2.4.2.30	Q9UKK3	*H. sapiens*	450
49	PARP6/8	PARP6	Poly [ADP-ribose] polymerase 6	2.4.2.30	Q2NL67	*H. sapiens*	175
50	PARP6/8	PARP8	Poly [ADP-ribose] polymerase 8	2.4.2.30	Q8N3A8	*H. sapiens*	175
51	PARP7/9-15	TIPARP	TCDD-inducible poly [ADP-ribose] polymerase	2.4.2.30	Q7Z3E1	*H. sapiens*	130
52	PARP7/9-15	PARP10	Poly [ADP-ribose] polymerase 10	2.4.2.30	Q53GL7	*H. sapiens*	130
53	PARP7/9-15	PARP11	Poly [ADP-ribose] polymerase 11	2.4.2.30	Q9NR21	*H. sapiens*	130
54	PARP7/9-15	PARP12	Poly [ADP-ribose] polymerase 12	2.4.2.30	Q9H0J9	*H. sapiens*	130
55	PARP7/9-15	PARP14	Poly [ADP-ribose] polymerase 14	2.4.2.30	Q460N5	*H. sapiens*	130
56	PARP7/9-15	PARP15	Poly [ADP-ribose] polymerase 15	2.4.2.30	Q460N3	*H. sapiens*	130
57	PARP7/9-15	PARP9	Poly [ADP-ribose] polymerase 9	2.4.2.30	Q8IXQ6	*H. sapiens*	130
58	PARP16	PARP16	Mono [ADP-ribose] polymerase	2.4.2.30	Q8N5Y8	*H. sapiens*	225
63	SIRT	SRT1	NAD-dependent protein deacetylase	3.5.1.-	Q9FE17	*A. thaliana*	180
64	SIRT	SRT2	NAD-dependent protein deacylase	3.5.1.-	Q94AQ6	*A. thaliana*	180
65	SIRT	sir-2.1	NAD-dependent protein deacetylase	3.5.1.-	Q21921	*C. elegans*	180
66	SIRT	sir-2.4	NAD-dependent protein deacetylase	3.5.1.-	Q95Q89	*C. elegans*	180
67	SIRT	sir-2.2	NAD-dependent protein deacylase	3.5.1.-	Q20480	*C. elegans*	180
68	SIRT	sir-2.3	NAD-dependent protein deacylase	3.5.1.-	Q20481	*C. elegans*	180
69	SIRT	SIRT1	NAD-dependent protein deacetylase sirtuin-1	3.5.1.-	Q96EB6	*H. sapiens*	180
70	SIRT	SIRT2	NAD-dependent protein deacetylase sirtuin-2	3.5.1.-	Q8IXJ6	*H. sapiens*	180
71	SIRT	SIRT3	NAD-dependent protein deacetylase sirtuin-3	3.5.1.-	Q9NTG7	*H. sapiens*	180
72	SIRT	SIRT4	NAD-dependent protein deacetylase sirtuin-4	3.5.1.-	Q9Y6E7	*H. sapiens*	180
73	SIRT	SIRT5	NAD-dependent protein deacetylase sirtuin-5	3.5.1.-	Q9NXA8	*H. sapiens*	180
74	SIRT	SIRT6	NAD-dependent protein deacetylase sirtuin-6	3.5.1.-	Q8N6T7	*H. sapiens*	180
75	SIRT	SIRT7	NAD-dependent protein deacetylase sirtuin-7	3.5.1.-	Q9NRC8	*H. sapiens*	180
76	SIRT	HST1	NAD-dependent protein deacetylase	3.5.1.-	P53685	*S. cerevisiae*	180
77	SIRT	HST2	NAD-dependent protein deacetylase	3.5.1.-	P53686	*S. cerevisiae*	180
78	Tankyrase	pme-5	Poly(ADP-ribose) polymerase	2.4.2.30	Q9TXQ1	*C. elegans*	150
79	Tankyrase	TNKS	Tankyrase-1	2.4.2.30	O95271	*H. sapiens*	150
80	Tankyrase	TNKS2	Tankyrase-2	2.4.2.30	Q9H2K2	*H. sapiens*	150
81	TRPT	emb1067	RNA 2'-phosphotransferase, Tpt1 / KptA family	2.7.1.160	Q9ZU32	*A. thaliana*	170
82	TRPT	TRPT1	tRNA 2'-phosphotransferase 1	2.7.1.160	Q86TN4	*H. sapiens*	170

Query proteins used for Blast searches.

Table S2

Name	ADPRcyc	ART	PARP1-3	PARP4	PARP6/8	PARP7/9-15	PARP16	SIRT	TRPT	Tankyrase	SUM
Mammalia	0.99	1.00	0.98	0.99	0.99	0.99	1.00	1.00	0.98	1.00	9.90
Hemichordata	1.00	0.00	1.00	1.00	1.00	1.00	1.00	1.00	1.00	1.00	9.00
Sauropsida	0.98	1.00	0.98	0.96	0.43	0.96	1.00	1.00	0.13	1.00	8.44
Neopterygii	0.92	0.24	0.96	0.88	0.72	0.76	0.96	0.96	0.84	0.96	8.20
Lophotrochozoa	0.80	0.00	1.00	1.00	0.80	0.80	1.00	1.00	0.80	1.00	8.20
Echinodermata	1.00	0.00	1.00	1.00	1.00	1.00	0.00	1.00	1.00	1.00	8.00
Branchiostoma	0.00	0.00	1.00	0.00	1.00	1.00	1.00	1.00	1.00	1.00	7.00
Cnidaria	1.00	0.00	1.00	1.00	1.00	0.00	0.50	1.00	0.50	1.00	7.00
Amphibia	0.67	0.67	0.67	0.67	0.67	0.33	0.67	0.67	0.33	0.67	6.00
Arthropoda	0.00	0.00	0.84	0.65	0.02	0.00	0.00	1.02	0.51	0.95	3.98
Platyhelminthes	0.00	0.00	1.00	0.00	0.33	0.00	0.00	1.00	0.50	1.00	3.83
Tunicata	0.00	0.00	1.00	0.00	0.00	0.00	0.00	1.00	0.00	1.00	3.00
Nematoda	0.00	0.00	1.00	0.00	0.00	0.00	0.00	1.00	0.00	1.00	3.00

Fraction of species with given NAD consumers per clade. For all clades at leaf positions in Figure 2B, the fraction of species in the respective clade possessing the respective NAD consumer is shown. For easier optical identification, table cell backgrounds are the darker, the higher the fraction is. The fraction of species with a given NAD consumer for clades that are not leaves is the sum of the values of all child nodes.

Table S3

Overview of kinetic constants used for the construction of the model.

Enzyme	EC number	Kinetic parameter	References	Rate Law
NADA	3.5.1.19	K_M:9.6μM K_{iP}:120μM k_{cat}:0.65s^{-1}	[2]	Product inhibition
NADS	6.3.5.1	K_M:190μM k_{cat}:21s^{-1}	[3]	HMM
NMNAT	2.7.7.1 2.7.7.18	$K_{M_{NaMN}}$:67.7μM $k_{cat_{NaMN}}$:42.9s^{-1} $K_{M_{NMN}}$:22.3μM $k_{cat_{NMN}}$:53.8s^{-1} $K_{M_{NAD}}$:59μM $k_{cat_{NAD}}$:129.1s^{-1} $K_{M_{NaAD}}$:502μM $k_{cat_{NaAD}}$:103.8s^{-1}	[4][1] [5][2] [5]	Substrate Competition
NNMT	2.1.1.1	$K_{M_{Nam}}$:400μM $K_{M_{SAM}}$:1.8μM K_{iP}:60μM k_{cat}:8.1s^{-1}	[6] [7]	Bi irreversible with product inhibition
NamPT	2.4.2.12	K_M:5nM k_{cat}:0.0077s^{-1} $K_{i_{NAD}}$: 2.1μM	[8]	Competitive inhibition
NAPRT	2.4.2.11	K_M:1.5μM k_{cat}:3.3s^{-1}	[8]	HMM
SIRT1	3.5.1.-	K_M:29μM K_{iP}:60μM k_{cat}:0.67s^{-1}	[9]	Product inhibition
NT5	3.1.3.5	$K_{M_{NaMN}}$:3.5mM $k_{cat_{NaMN}}$:2.8s^{-1} $K_{M_{NMN}}$: 5mM $k_{cat_{NMN}}$:0.5s^{-1}	[10]	HMM
PNP	2.4.2.1	K_M:1.48mM k_{cat}:40s^{-1}	[11]	HMM
NRK	2.7.1.173	K_M:3.4μM k_{cat}:0.23s^{-1}	[12]	HMM

Additional parameter and model description

The total enzyme concentration was set to 10 times the scaling factor, for all enzymes except NamPT and NADA. For NamPT the concentration was set to 400 times the scaling factor if not stated otherwise. For NADA the enzyme concentration was set to 400 times the scaling factor in the model used for Figure 6 and S6 and to 0 otherwise. As enzyme concentrations here have an arbitrary unit, a scaling factor of 0.1μM was applied to all enzymatic reactions to achieve consumption rates that are in the range of reported values [13]. Concentration of potential co-substrates except SAM were assumed to be constant and not-limiting for the reaction. If not stated otherwise, the SAM concentration was set to 80 μM refelecting the concentration of SAM in liver tissues [14]. Thus being implicitly represented by maximal velocities consisting of total enzyme concentration times turnover rates. Nam import rates for import into the system was set to 0.1 μM/s for all simulations, being in the range measured for Nam uptake in mammalian cells [15]. In addition to the reactions listed above an additional NAD consumption was simulated using HMM-kinetics with a substrate affinity of 0.3 mM and a turnover rate of 1. Furthermore, reversible NAD binding to proteins was simulated using reversible mass actions kinetics with an equilibrium constant of 0.1, which is in a range of values reported in the literature, dissociation and association constants where set to 10 and 100s^{-1} respectively. For the two compartment simulation, compartment size was equal for both compartments and set to 1μl. The actual compartment size does

[1] Values for NMNAT1 used
[2] Equilibrium constant used for calculation of turnover rate of reverse reaction

not change the outcome of the simulations as long as both compartments have equal volumes. The Nam import rates were set to $100s^{-1}$ for both compartments. The amount of NADA present was set to 400. Thus equal to the amount of NamPT used.

To account for cell growth, we added an outflow reaction to each simulated metabolite. For this reaction we simulated a constant flux based on mass action kinetics. The reaction rate was equal for each metabolite and simulated to be in a range between $2.7 \cdot 10^{-6} s^{-1}$ and $2.8 \cdot 10^{-5} s^{-1}$, corresponding to a doubling in volume once every 0.01 to 1 hour, denoted as cell division rate in Figure 3.

Rate Laws referred to in Table S3

Product inhibition

$$v = \frac{E_T \cdot k_{cat} \cdot S}{K_M + S + \frac{K_M \cdot P}{K_{iP}}} \tag{1}$$

Bi irreversible with product inhibition

$$v = \frac{E_T \cdot k_{cat} \cdot A \cdot B}{K_{ma}(1 + \frac{P}{K_{iP}})(B + K_{mb}) + A \cdot K_{mb}} \tag{2}$$

Competitive inhibition

$$v = \frac{E_T \cdot k_{cat} \cdot S}{K_M + S + \frac{K_M \cdot I}{K_{iI}}} \tag{3}$$

Henry-Michaelis Menten for irreversible reactions (HMM)

$$v = \frac{E_T \cdot k_{cat} \cdot S}{K_M + S} \tag{4}$$

Substrate competition at NMNAT

$$v = E_T \cdot \frac{\frac{k_{cat_A} \cdot A \cdot B}{K_{M_A}} - \frac{k_{cat_P} \cdot P \cdot Q}{K_{M_P}}}{1 + \frac{A}{K_{M_A}} + \frac{B}{K_{M_B}} + \frac{P}{K_{M_P}} + \frac{Q}{K_{M_Q}}} \tag{5}$$

Table S4

PDB Code	2H3D	3DGR	3DHD	3DHF	3DKJ	3DKL
2H3D	-	0.95	0.85	0.86	0.88	0.88
3DGR		-	0.61	0.61	0.55	0.57
3DHD			-	0.43	0.40	0.43
3DHF				-	0.42	0.33
3DKJ					-	0.39
3DKL						-

Root mean square deviation (RMSD) values between different structures (in Å). The alignment and RMSD calculation was done with PyMOL[16]. The structures are 2H3D (human NAMPT) [17], 3DGR (human NAMPT·AMPcP complex) [18], 3DHD (human NAMPT·NMN·Mg_2PPi complex) [18], 3DHF (human BeF_3^--NAMPT·NMN·Mg_2PPi complex) [18], 3DKJ (human NAMPT·PRPP·BzAM complex) [18], and 3DKL (human BeF_3^--NAMPT·Mg_2PRPP·BzAM complex) [18]. The structural resolution of the PDB structures ranges from 1.8 Å to 2.1 Å.

References

[1] Prum RO, et al. (2015) A comprehensive phylogeny of birds (aves) using targeted next-generation dna sequencing. *Nature* 526(7574):569–73.

[2] Smith BC, et al. (2012) Structural and kinetic isotope effect studies of nicotinamidase (Pnc1) from saccharomyces cerevisiae. *Biochemistry* 51(1):243–256.

[3] Yi CK, Dietrich LS (1972) Purification and properties of yeast nicotinamide adenine dinucleotide synthetase. *Journal of Biological Chemistry* 247(15):4794–4802.

[4] Sorci L, et al. (2007) Initial-rate kinetics of human NMN-adenylyltransferases: Substrate and metal ion specificity, inhibition by products and multisubstrate analogues, and isozyme contributions to NAD+ biosynthesis. *Biochemistry* 46(16):4912–4922.

[5] Berger F, Lau C, Dahlmann M, Ziegler M (2005) Subcellular compartmentation and differential catalytic properties of the three human nicotinamide mononucleotide adenylyltransferase isoforms. *Journal of Biological Chemistry* 280(43):36334–36341.

[6] Aksoy S, Szumlanski CL, Weinshilboum RM (1994) Human liver nicotinamide N-methyltransferase. cDNA cloning, expression, and biochemical characterization. *Journal of Biological Chemistry* 269(20):14835–14840.

[7] Alston TA, Abeles RH (1988) Substrate specificity of nicotinamide methyltransferase isolated from porcine liver. *Archives of biochemistry and biophysics* 260(2):601–608.

[8] Burgos ES, Schramm VL (2008) Weak coupling of ATP hydrolysis to the chemical equilibrium of human nicotinamide phosphoribosyltransferase. *Biochemistry* 47(42):11086–11096.

[9] Borra MT, Langer MR, Slama JT, Denu JM (2004) Substrate Specificity and Kinetic Mechanism of the Sir2 Family of NAD + -Dependent Histone/Protein Deacetylases †. *Biochemistry* 43(30):9877–9887.

[10] Kulikova V, et al. (2015) Generation, release, and uptake of the NAD precursor nicotinic acid riboside by human cells. *Journal of Biological Chemistry* 290(45):27124–27137.

[11] Wielgus-Kutrowska B, Kulikowska E, Wierzchowski J, Bzowska A, Shugar D (1997) Nicotinamide riboside, an unusual, non-typical, substrate of purified purine-nucleoside phosphorylases. *European Journal of Biochemistry* 243(1-2):408–414.

[12] Dölle C, Ziegler M (2009) Application of a coupled enzyme assay to characterize nicotinamide riboside kinases. *Analytical Biochemistry* 385(2):377–379.

[13] Liu L, et al. (2018) Quantitative analysis of NAD synthesis-breakdown fluxes. *Cell Metabolism* 27(5):1067–1080.e5.

[14] Reed MC, Nijhout HF, Sparks R, Ulrich CM (2004) A mathematical model of the methionine cycle. *J Theor Biol* 226(1):33–43.

[15] Billington RA, et al. (2008) Characterization of nad uptake in mammalian cells. *J Biol Chem* 283(10):6367–74.

[16] Schrödinger, LLC (2010) The {PyMOL} Molecular Graphics System, Version˜1.4.1.

[17] Wang T, et al. (2006) Structure of Nampt/PBEF/visfatin, a mammalian NAD+ biosynthetic enzyme. *Nature Structural & Molecular Biology* 13(7):661–662.

[18] Burgos ES, Ho MC, Almo SC, Schramm VL (2009) A phosphoenzyme mimic, overlapping catalytic sites and reaction coordinate motion for human NAMPT. *Proceedings of the National Academy of Sciences* 106(33):13748–13753.